Optical and Quantum Electronics (2020) 52:393
https://doi.org/10.1007/s11082-020-02472-9

Design of a human eye retinal camera optical system with dual-wavelength coaxial astigmatism correction

Duo Wang[1,2] · Rui Ouyang[1,2] · Guoling Bi[1] · Longxu Jin[1] · Xingxiang Zhang[1]

Received: 1 April 2020 / Accepted: 6 July 2020 / Published online: 28 August 2020

Abstract
In order to better improve vision, an accurate measurement of the aberrations in the human eye has important experimental and clinical significance. An adaptive fundus camera that uses a double-column lens to correct human astigmatism is designed. In the illumination system, ring light generated by a pair of axicon lenses is used to illuminate the human eye, abandoning the traditional illumination method. In the target adjustment system, a simple real image is set, the plane mirror group and the double cylinder lens are adjusted, and the defocus and astigmatism of the human eye are corrected, so that the residual aberration of the human eye is controlled within the correction range of the adaptive imaging system. In the adaptive imaging system, a Shack–Hartmann wavefront sensor is used as a wavefront detector, and a liquid crystal spatial light modulator is used as a wavefront corrector to correct the high-order aberrations of the human eye. The lighting system and imaging system operate in different bands. The simulation results show that the illumination light path avoids the strongly reflected light of the cornea and can uniformly illuminate the human eye. The design of the adaptive imaging system achieves the diffraction limit, and the astigmatism is corrected by a cylindrical lens in the imaging system. Additional aberrations are generated, and the plane mirror is adjusted to adjust the optical path to accommodate human eyes with different diopters.

Keywords Human eye · Fundus camera · Illumination system · Adaptive imaging system

1 Introduction

The human brain obtains information from the outside world through five senses every day. Researchers at Harvard Business School in the United States have shown that the proportion of visually accepted information reaches 83%. A natural scene forms an inverted real

✉ Duo Wang
wangduo161@mails.ucas.ac.cn

[1] Changchun Institute of Optics, Fine Mechanics and Physics, Chinese Academy of Sciences, Changchun 130033, China

[2] University of Chinese Academy of Sciences, Beijing 100049, China

image on the retina through the optical system of the human eye. The human eye is an extremely complex optical system that is intelligent but not perfect (Smith 2008) . When the human eye is stimulated by external light, the internal refractive medium, surface curvature and thickness will vary from person to person. Many animals, including humans, inherently experience refractive errors, which means that the axial length and power of the eye do not match (Yau et al. 2012). In addition, many human diseases, such as diabetes and hypertension, can cause retinopathy (Zhang et al. 2019; Ogagarue et al. 2013). Because the blood vessels in the retina are the only observed blood vessels in the whole body, fundus photographs are the gold standard for judging the characteristics of diseases (Kaizu et al. 2019). Even a normal human eye cannot avoid a certain aberrations, and the existence of human eye aberrations not only affects the visual resolution but also affects the image quality of the fundus. Therefore, the design of a human fundus imaging camera not only needs to correct human eye aberrations but also needs to consider the differences in the human eye.

The two prominent features of human eye aberrations are crowd dispersal and amplitude fluctuations. The correction of the human eye aberration caused by crowd differences and the improvement of the application range of the high-resolution imaging technology of the retina is the biggest problem in clinical applications. The current popular practice is to correct low-order aberrations and high-order aberrations separately and to relax the requirements of the wavefront aligner for fundus imaging systems (Suliman and Rubin 2019; Krueger et al. 2016). For the lower-order aberrations, the easiest way is to insert an optometry sheet to compensate for the abberations (Manny et al. 2016; Chen et al. 2007); however, one of the problems with this approach is the reduction in the passage of light energy, and another problem is the change in the conjugate relationship between the human pupil, wavefront detector and wavefront corrector, which adversely affects the accuracy of the aberration correction. In addition, the degree of compensation of the optometry sheet is discontinuous, and a full compensation for low-order aberrations cannot be achieved. Higher-order aberrations cannot be corrected with conventional spherical and cylindrical mirrors (Planchon et al. 2003) but can be corrected using excimer laser correction techniques and adaptive optics techniques (Niparugs et al. 2018; Sun et al. 2012). Affected by many factors, the effect of excimer laser correction technology in correcting the high-order aberrations of human eyes is not ideal, and adaptive optics has been successfully applied to human fundus imaging (Qin et al. 2020; Chen et al. 2006). However, adaptive optics has a certain correction range due to the limitations of the wavefront corrector.

When light from the external environment enters the inside of the human eye through the pupil, although the retina of the fundus can be illuminated, the energy is not strong enough to be used to clearly image the fundus of the human eye. Moreover, the reflected light of the cornea of the human eye is too strong relative to the brightness of the fundus (Han et al. 2002) , which is very unfavorable for imaging the fundus. Therefore, to be able to clearly image the fundus, it is necessary to design a lighting system that can illuminate the fundus while avoiding a strong corneal reflection. Currently, the common practice is ring light illumination and polarizer (PBS) extinction (Ma et al. 2014; Ye et al. 2013). However, both methods have obvious disadvantages. The traditional method of generating ring light is to use a ring diaphragm, but the center of the ring diaphragm will produce an occlusion, and the utilization of light energy will be reduced; when a polarizing device (PBS) is used to eliminate the stray light reflected by the cornea, since only the polarized light of one polarization direction in the light reflected by the retina can be utilized, the energy loss is severe.

2 Principle

2.1 Rotating double cylindrical mirror for astigmatism correction

When people use the eye in a nonstandard manner, the eye may have different powers in the meridional direction and the sagittal direction. Compared with other directions, human eye has a stronger radius of action in one direction; that is, the convergence of light is stronger. The phenomenon of astigmatism is formed in optics, and in medicine, it is commonly called astigmatism. In a clinical correction, the correction can be achieved by introducing the same amount of astigmatism in the direction of the vertical axis. Rotating double cylindrical mirrors consist of two cylindrical mirrors with the same focal length. By adjusting the relative angle between the two cylindrical mirrors and the overall rotation, the astigmatism in the axis and the size can be specified to achieve astigmatism compensation for human eyes.

Sauders (1980) proposed the use of the defocus Q_S,the astigmatism Q_A an axis *theta* to represent the refraction of a medical imaging system, which can also be used to describe the imaging. The diopter of a single cylindrical mirror can be expressed as Q_S,$Q_A \times \theta$, where $Q_S = 0$,Q_A represents the magnitude of the diopter of a single cylindrical mirror, and *theta* indicates the angle at which the cylindrical mirror rotates. To facilitate the calculation of the diopter of a synthetic double cylindrical mirror, the traditional medical expression is now converted into matrix form:

$$Q = \begin{pmatrix} Q_s + Q_A \sin^2\theta & Q_A \sin\theta\cos\theta \\ -Q_A \sin\theta\cos\theta & Q_S + Q_A \cos^2\theta \end{pmatrix} \tag{1}$$

In matrix form, the diopter expression of the double cylindrical mirror can be obtained by adding the matrix expressions of the single cylindrical mirror, which can be expressed simply $Q_D = Q_1 + Q_2$, This is a matrix expression of the diopter of the synthesized double cylindrical mirror. The expanded form is as follows:

$$Q_D = \begin{pmatrix} Q_{11} & Q_{12} \\ Q_{21} & Q_{22} \end{pmatrix} \tag{2}$$

$$Q_{11} = Q_{S1} + Q_{S2} + A\sin^2\theta_2 \tag{3}$$

$$Q_{11} = -Q_{A1}\sin\theta_1\cos\theta_1 - Q_{A2}\sin\theta_2\cos\theta_2 \tag{4}$$

$$Q_{21} = -Q_{A1}\sin\theta_1\cos\theta_1 - Q_{A2}\sin\theta_2\cos\theta_2 \tag{5}$$

$$Q_{22} = Q_{S1} + Q_{S2} + Q_{A1}\cos^2\theta_1 + Q_{A2}\cos^2\theta_2 \tag{6}$$

The parameters of the double cylindrical mirror are $Q_{S1} = Q_{S2} = 0, Q_{A1} = Q_{A2} = Q_A$. Substituting (3), (6) and then converting the traditional medical expression into the expression for a double cylindrical mirror Q_{SD},$Q_{AD} \times \varphi$,the specific form is as follows:

$$Q_{SD} = 2Q_A \sin^2\left(\frac{\theta_1 - \theta_2}{2}\right) \tag{7}$$

$$Q_{AD} = 2Q_A \cos\left(\theta_2 - \theta_1\right) \tag{8}$$

$$\varphi = \frac{\theta_1 + \theta_2}{2} \tag{9}$$

(7)–(9) constitute the medical formulae for correcting astigmatism with a double cylindrical mirror, where Q_{SD} indicates the amount of defocus of the double cylindrical mirror, Q_{AD} represents the astigmatism component of the double cylindrical mirror, and φ indicates the astigmatic axis of the double cylindrical mirror. Thus, the double cylindrical mirror rotation angles θ_1 and θ_2 form a relationship between the astigmatism size and axial angle.

2.2 Principle of the axicon lens pair

The working principle of the axicon lens group is shown in Fig. 1.

r_1 is the radius of the incident beam, r_2 is the radius of the inner ring of the ring illumination, d is the distance between the two axicon lenses, and α is the cone angle. The characteristic feature of the axicon lens is that the resulting annular illumination ring width is constant and always equals r_1. The adjustment distance d can be continuously adjusted by δ . The adjustment of the axicon lens via δ is described in the literature (Rioux et al. 1978) but only for a given $\alpha$and a beam magnification below 10°. The approximate formula for M is:

$$M \approx 1 + \frac{d\alpha}{r_1}\left(\frac{n-1}{1-\alpha}\right), \alpha < 10^\circ \tag{10}$$

The above formula has an approximation error due to the trigonometric function, and the range of α is limited. The formula for the exact magnification M is deduced below. From the geometric relationship in the Fig. 1., the magnification of the axicon lens group is:

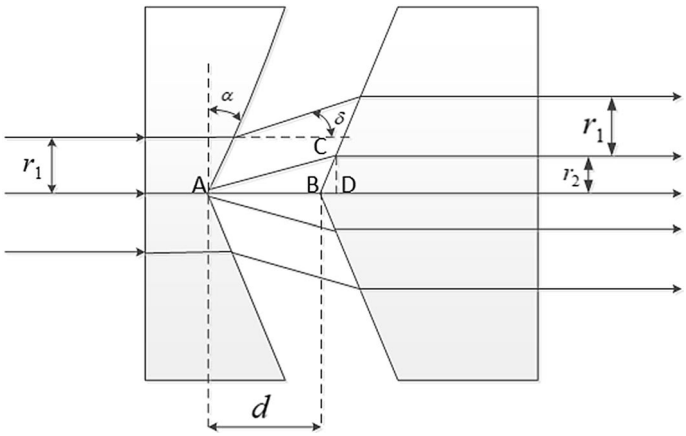

Fig. 1 Schematic diagram of the axicon lens group

$$M_{real} = \frac{r_1 + r_2}{r_1} = 1 + \frac{BC \cdot \cos(\angle BCD)}{r_1} = 1 + \frac{BC \cdot \cos\alpha}{r_1} \tag{11}$$

Applying the cosine theorem to the triangle ABC:

$$\frac{AB}{\sin(\angle BCA)} = \frac{BC}{\sin(\angle CAB)} \tag{12}$$

Snell's law is

$$n \sin\alpha = \sin' \alpha \tag{13}$$

Deriving the exact magnification of the axicon lens:

$$M_{real} = \frac{r_1 + r_2}{r_1} = 1 + \frac{d}{r_1}\left(\frac{n \sin\alpha \cos^2\alpha}{\sqrt{1 - n^2 \sin^2\alpha}} - \sin\alpha \cos\alpha\right) \tag{14}$$

Therefore, the inner diameter of the ring light is:

$$r_2 = \frac{d \tan[\arcsin(n \sin\alpha) - \alpha]}{1 - \tan\alpha \tan[\arcsin(n \sin\alpha) - \alpha]} \tag{15}$$

As can be seen from the above formula, there is a linear relationship between the inner diameter of the ring beam r_2 and the distance between the two axicon lenses d , which is advantageous for controlling the inner diameter of the annular beam via the corner step of the cam driving motor. Compared with the conventional annular diaphragm, the annular beam generated by the axicon lens group has no central obstruction and a high energy utilization.

2.3 System structure and working principle

The designed retinal camera system for dual-wavelength coaxial astigmatism correction consists of the camera system shown in Fig. 2. The entire system consists of three parts: the target adjustment system, the illumination system, and the adaptive imaging optics. In the illumination system, 790 nm near-infrared light with a high retinal reflectance by the human eye that induces a small stimulation to the human eye is selected, and in the adaptive imaging system, 570 nm visible light with good contrast in blood vessels is selected. The 570 nm visible light will achieve a higher resolution limit than the near-infrared light. As can be seen from the Fig. 2, the illumination system and the imaging system share the lens L4, and a coaxial optical path is used to illuminate the fundus retina. The purpose of coaxial optical path is to improve the illumination quality. In the adaptive imaging optical path, a Shack–Hartmann wavefront sensor is used to detect the wavefront aberration, and a liquid crystal spatial light modulator is used as a wavefront corrector.

The working process of the system is as follows: light emitted by a He-Ne laser with a wavelength of 632.8 nm is expanded and then focused by the lens L1 into the reticle. The reticle is used as the target, and then the light passes through the conjugate lens group L2 and L3 to form the first image. At the filtering aperture H1, the purpose of the real image is to achieve focusing. When the human eye gazes at the real image at H1, the fundus retina image passes through the double-column lens group C1 and C2, the lens L4, and the plane

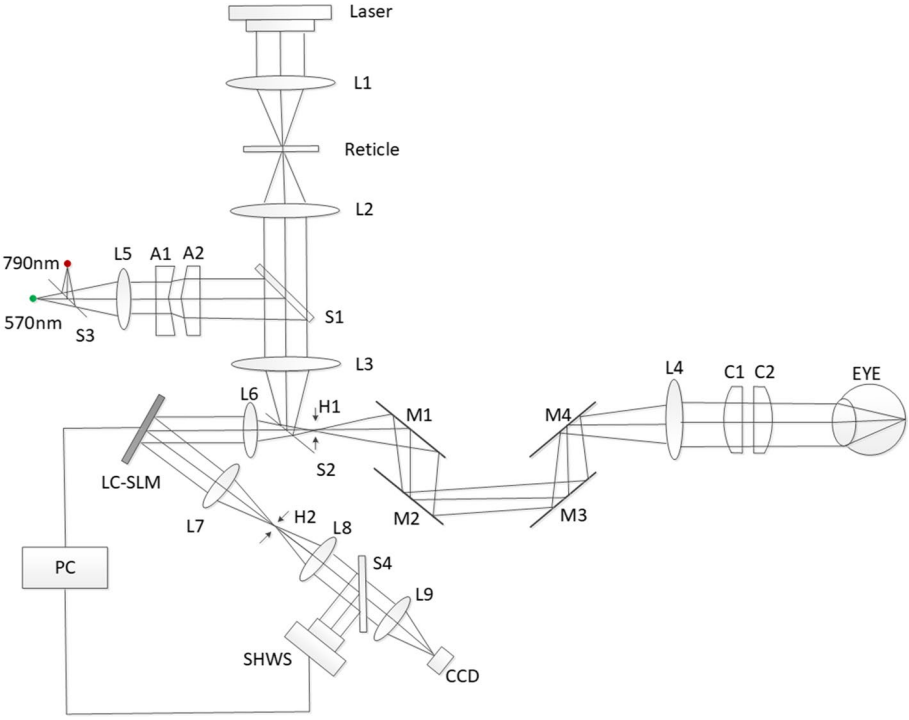

Fig. 2 Schematic diagram of human eye accommodation fundus camera

mirror group M1 to M4; by adjusting the rotation angle of the double-column lens group and the distance between the plane mirror groups M1 and M2 (the distance between M3 and M4 is equivalent to that between M1 and M2), the human eye can see the image of the reticle, and the primary aberration of the human eye is basically corrected.

The structure of the plane mirror group is shown in Fig. 3. The main function is to help the human eye focus, and the other function is to shorten the light path, ensuring that the eye can always see the real image at the small hole H1 and that the eye is always imaged at the filter aperture H1.

The detecting light source emits near-infrared light at 790 nm, which sequentially passes through the beam expanding mirror L5 of the illumination system, the axicon mirrors A1 and A2, the dichroic mirror S1, the lens L3, the dichroic mirror S2, the first filtering aperture H1, and the plane mirror group M1 to M4, the lens L4, and the cylindrical lenses C1 and C2 to illuminate the human eye. The reflected light of the fundus of the human eye with aberrations is emitted through the human eye and sequentially passes through the cylindrical lenses C2 and C1, the lens L4, the plane mirror group M4, M3, M2, and M1, the first filtering aperture H1, the dichroic mirror S2, the collimating mirror L6, the liquid crystal spatial light modulator, the focusing mirror L7, the second filtering aperture H2, and the collimating mirror L8; the light is then reflected by the half-mirror S4 to the SHWS to detect the wave aberration of the human eye, which is fed back to a personal computer (PC). The detected wavefront information is then processed by the computer to obtain a control signal, which is sent to the LC-SLM for wavefront correction. Finally, a light

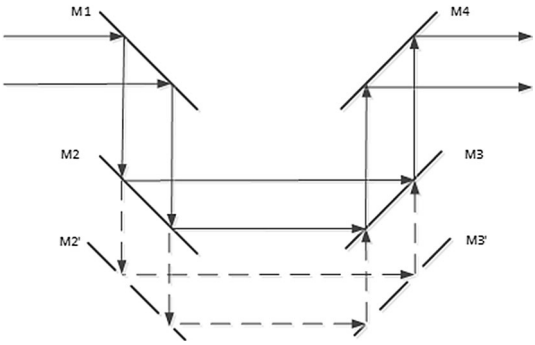

Fig. 3 Schematic diagram of working mode of plane mirror group: adjust the optical path by moving the positions of plane mirrors 2 and 3 at the same time

source emits visible light with a wavelength of 570 nm, which illuminates the fundus of the human eye through an illumination path (in the same order as the near-infrared light). The reflected light from the fundus of the human eye in turn passes through the adaptive imaging optical path and is imaged on the CCD detector. The axicon lenses A1 and A2 of the illumination optical system convert the illumination light into ring-shaped light with an adjustable inner diameter to illuminate the cornea of the human eye, avoiding the strong central region of the reflected light and uniformly directing the beam to the fundus of the human eye.

3 Optical system design

3.1 Parameter design

Entrance pupil: the entrance to the imaging system selects the pupil of the human eye. The diameter of the pupil of the human eye under normal conditions is 2–7,mm, and the entrance pupil is 6 mm without dilation;

Wavelength: detection wavelength: 790 nm, imaging wavelength: 570 nm;
Imaging field of view angle: 2°;
Retinal resolution: 2.6 μm;
CCD pixel size: 6.5 μm;
Magnification: 5;
Total length of the system: no more than 300 mm.

3.2 Target system

The purpose of the design of the target adjustment system is to be able to focus the human eye. By adjusting the distance between the plane mirror groups, the primary aberration of the human eye due to myopia or far vision is corrected, and the chromatic aberration caused by the difference between the detection wavelength and the imaging wavelength is adjusted. The optical path diagram of the system is shown in Fig. 4.

The model imaged at H1 is established in CODE V, as shown in Fig. 5.The light source has a wavelength of 632.8 nm, and the target is a glass plate of a cross-hair, and the object height is 1 mm.

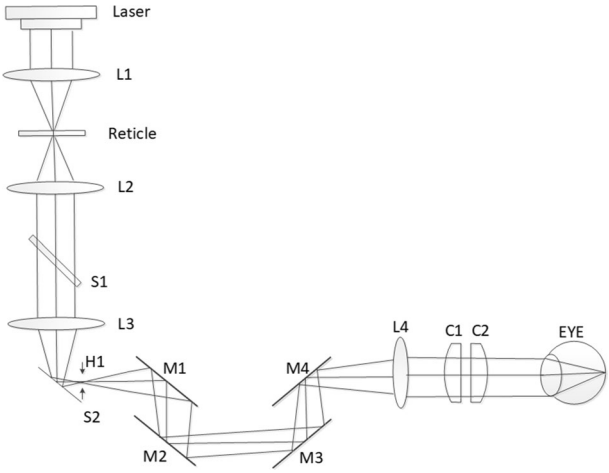

Fig. 4 Target adjustment system structure

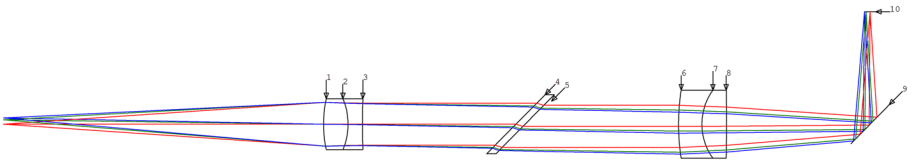

Fig. 5 Target imaging optical path simulation

In order to ensure that the human eye can clearly see the image of the target, and it is easy to adapt to the adjustment of the eye of different human eyes, it is required that the image formed at H1 should have good image quality, the design resultis shown in Fig. 6. It can be seen from the Fig. 6 that the aberration curve of the image formed by the target adjustment system at H1 is less than 10μm, the root mean square (RMS) radius of the spot diagram is less than 0.8 μm, and the MTF reaches the diffraction limit.

3.3 Lighting system

The illumination system adopts the structure of the axicon group to produce the annular light with adjustable inner diameter to adapt to different human eyes. The optical path structure is shown in Fig. 7a, and the design is shown in Fig. 7b. Near infrared light of 790 nm with less stimulation to human eyes was chosen as illumination source, and the glass material of the axicon was selected from the common NBK7 optical glass. Using the optical model of the classic Gullstrand–Le Grand eye (Fülep et al. 2019; Huanqing et al. 2005), see Fig. 8, using the lighttools software to simulate the entire lighting system. In lighttools, the light source is set to Vol Cyl Source, the power is 10 W, the number of light is 100,000, the inner diameter of the cornea at the cornea is 3 mm, and the outer diameter is 7 mm. The generated annular light avoids the central area where the reflected light is strong and enters the human eye from the edge of the cornea. Figure 9a shows the illumination effect of the annular spot and Fig. 9b shows the illumination energy distribution at the cornea.

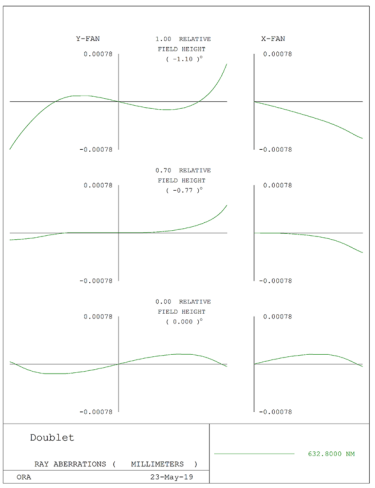

(a) aberration curve

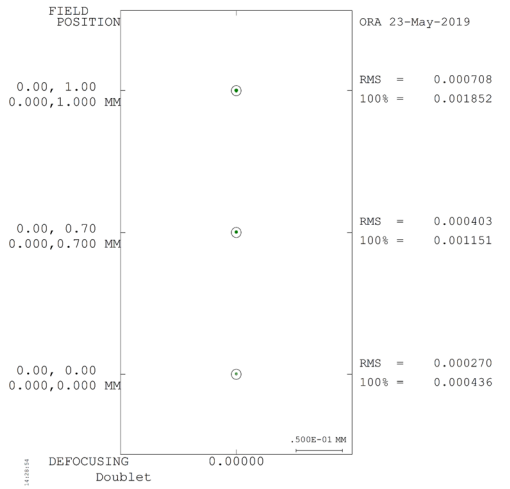

(b) spot diagram

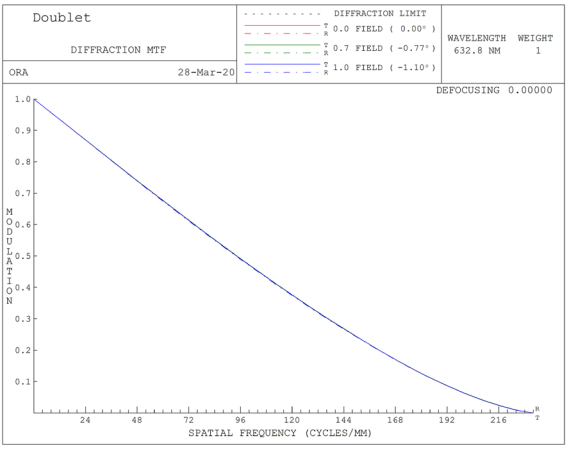

(c) MTF

Fig. 6 Design results of target imaging optical path simulation

3.4 Imaging system

For an ideal human eye, light reflected through the fundus will be emitted in parallel light. On the basis of the human eye without aberration, the adaptive imaging system is simulated by CODE V, in which the liquid crystal spatial light modulator is replaced by a plane mirror, and the optical path structure diagram is shown in Fig. 10a, and the design result is shown in Fig. 10b.

The human eye cannot be ideal, and there will inevitably be aberrations. However, after focusing by the plane mirror group and the double-column lens, the residual of the human eye will become very small. So in software design, plane mirror instead of liquid crystal spatial light modulator is chosen to correct aberration. On the one hand, the plane mirror group M1–M4 can shorten the optical path,on the other hand, by adjusting M2 and M3,

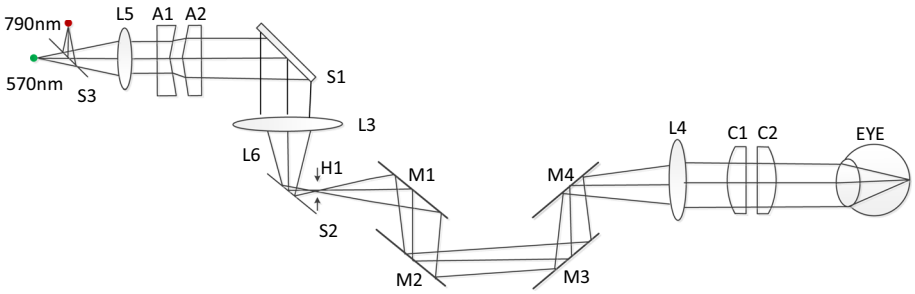

(a) lighting system optical path structure

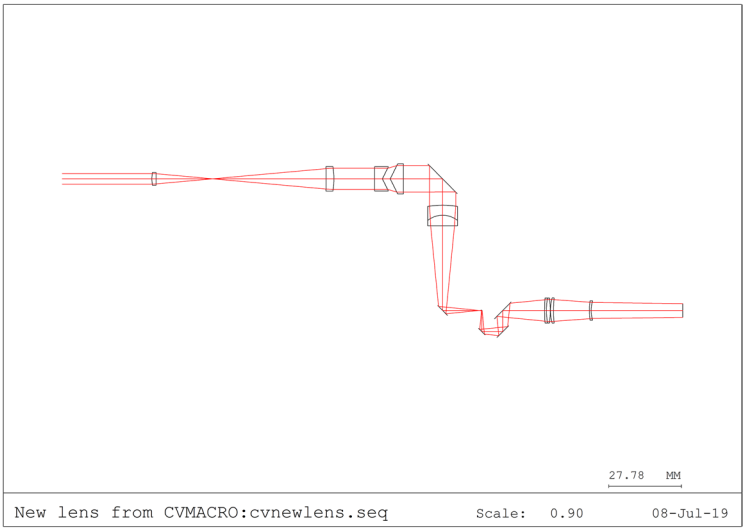

(b) optical simulation of illumination light path

Fig. 7 Schematic diagram of illumination light path and actual optical simulation

the human eye with farsightedness or myopia can always be imaged at H1; by adding the cylindrical lenses C1 and C2, the person with astigmatism can be adjusted. filter holes are provided at H1 and H2, which can effectively eliminate the influence of stray light on the imaging quality of human eyes; LC-SLM is tilted at a certain angle, which plays the role of folding the optical path to shorten the total length of the system.

Figure 11 shows the final result of the design. The dot spot of the spot diagram is smaller than the diffraction limit, the transfer function of the field of view is also close to the diffraction limit. The MTF at 77 lp/mm at Nyquist is greater than 0.42, which is in line with the requirements of a CCD using 6.5 µm pixels. Moreover, the field curvature of the imaging system is less than 0.08 mm, and the full field of view distortion is less than 0.15%, which ensures that the imaging effect is not distorted.

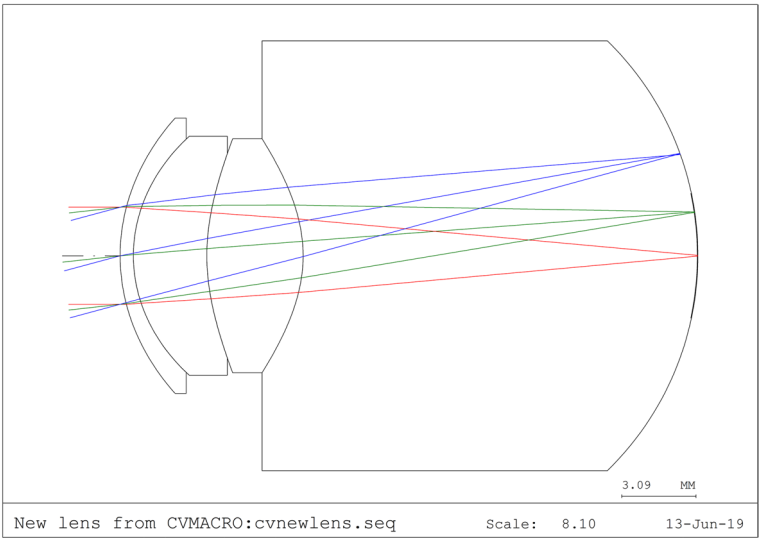

Fig. 8 Optical model of the Gullstrand–Le Grand eye

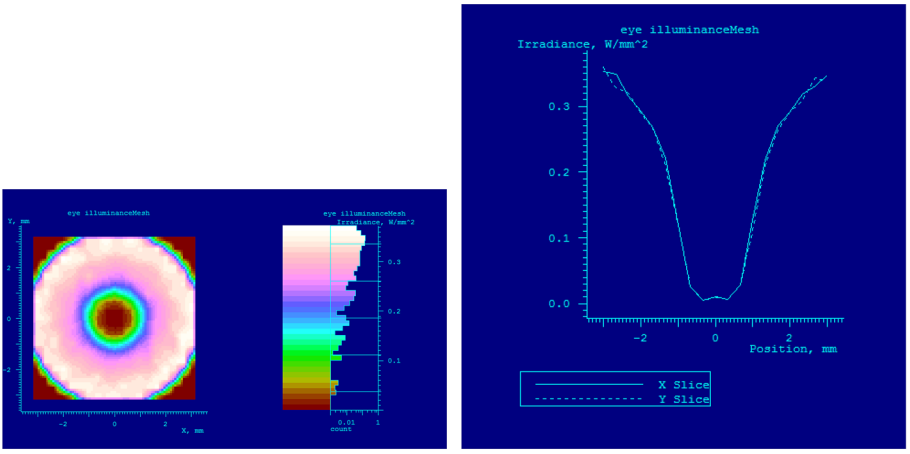

(a) illumination annulus at the pupil of the eye

(b) distribution of illumination energy at the cornea

Fig. 9 Simulation of illumination uniform by lighttools

4 Simulated human eye aberration compensation

Taking the human eye as an experimental object, the measured uncorrected Zernike coefficients are input one-to-one into the imaging system, that is, artificially introduced into the wavefront.Then, the Zernike coefficient is used to calculate the defocus, astigmatism and

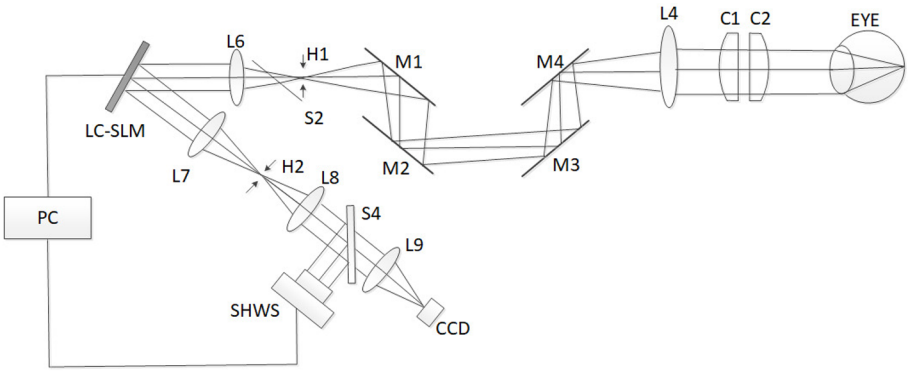

(a) adaptive imaging optical path structure

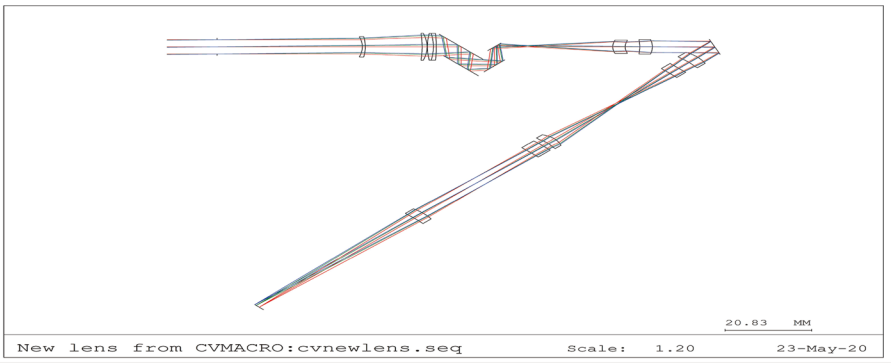

(b) adaptive imaging system simulation

Fig. 10 Schematic diagram and actual optical simulation of adaptive imaging optical system

axial angle of the human eye, and then the rotation angle of the two cylindrical lenses can be obtained. The astigmatism of the human eye is corrected by the cylindrical lens, and the distance compensation between the planar mirror groups M1 and M4 is adjusted. If the focusing range of M1~M4 is limited, defocusing can be introduced by using cylindrical lens to correct astigmatism, and defocusing can be compensated by combining plane lens group and cylindrical lens.

The experiment of simulating human astigmatism is carried out. Only the Zernike coefficient term corresponding to the astigmatism is input (Fink and Micol 2006), and the wavefront simulation at the entrance is performed in code V and MATLAB, respectively. Figure 12 is an astigmatic wavefront aberration diagram introduced at the entrance pupil, and Fig. 13 is a wavefront aberration showing the image plane in CODE V.

According to the diopter formula, the defocus, astigmatism and axial directions are calculated. Then, according to the Sect. 2.1, the relevant parameters of the cylindrical lens are obtained, and the optical software CODE V is input to simulate the wavefront. The wavefront aberration correction result of the image plane is shown in Fig. 14. Before the uncorrected, the wavefront root mean squarethe (RMS) is 1.41λ ,after correcting with the cylindrical lens, the RMS is 0.04λ , which achieves a good correction effect. The Fig. 15 shows the variation of the

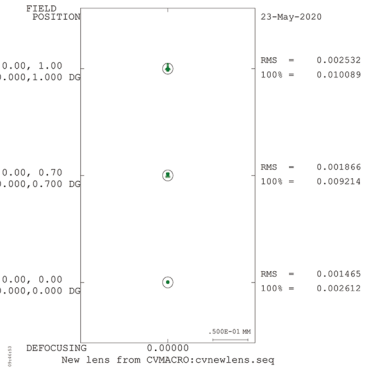

(a) spot diagram

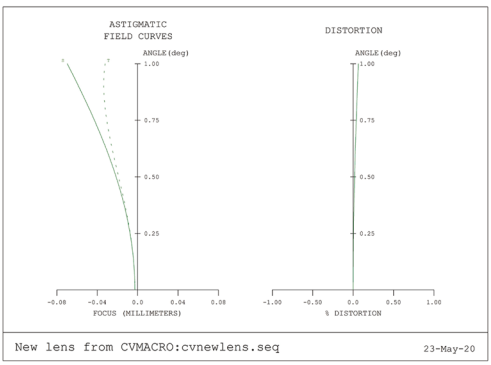

(b) ray aberration curves

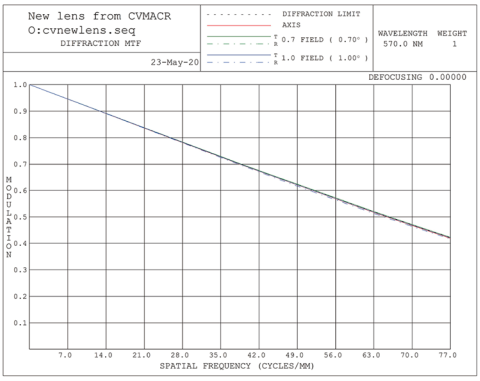

(c) MTF

Fig. 11 Design result of imaging system optical path simulation

Zernike coefficient that introduces the wavefront aberration and corrects the first 15 terms of the introduced aberration. By adjusting the double-column lens, it can be seen that the corrected results of the fourth and sixth terms of the astigmatism are basically close to 0, the fifth term is the defocus term. It is apparent from Fig. 15 that the change after the correction is also small, and is close to 0. The variation of the aberrations of other orders is small, indicating that the astigmatism is corrected by the cylindrical mirror. At the same time, no additional aberrations are introduced, which greatly reduces the dynamic range of the Shack–Hartmann wavefront sensing.

5 Conclusions

Faced with the problem of human eye aberration caused by population differences, the application of fundus camera to the population is expanded. A method is designed to correct the primary aberration of human eyes by adjusting the distance between the flat lens groups and the rotation angle between the cylindrical lenses, so that the residual aberration can be within the scope of the adaptive optical system. In addition, the illumination system

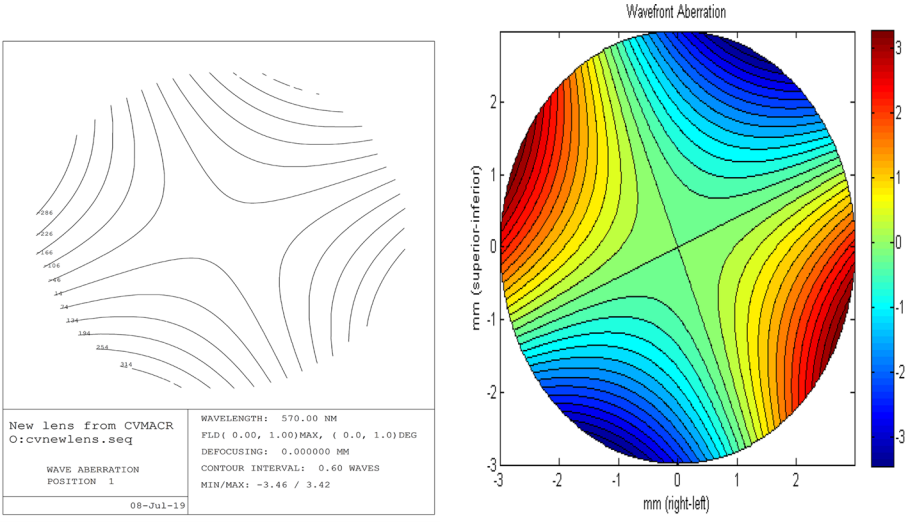

(a) wavefront simulated by CODE V **(b)** wavefront simulated by MATLAB

Fig. 12 Experimental wavefront aberration simulation of astigmatism in human eyes with Zernike term coefficient

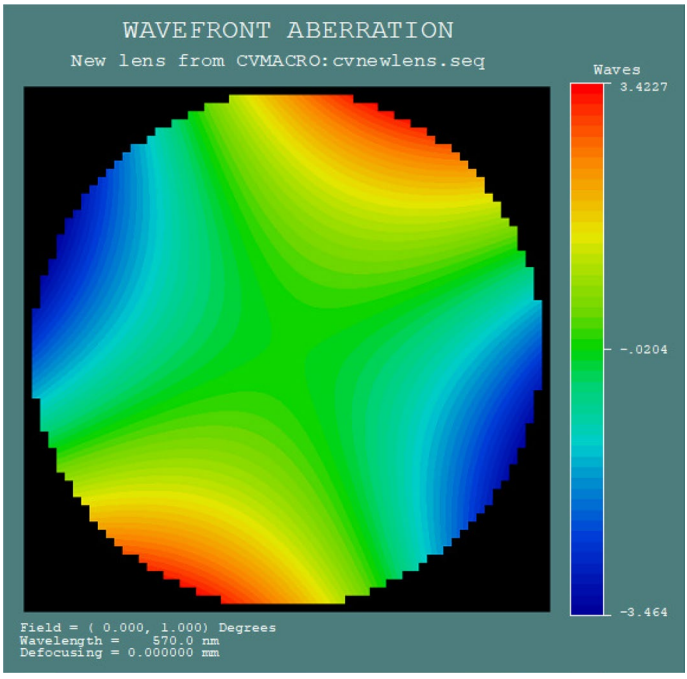

Fig. 13 Wavefront aberration diagram on the image plane after astigmatism is introduced in code V

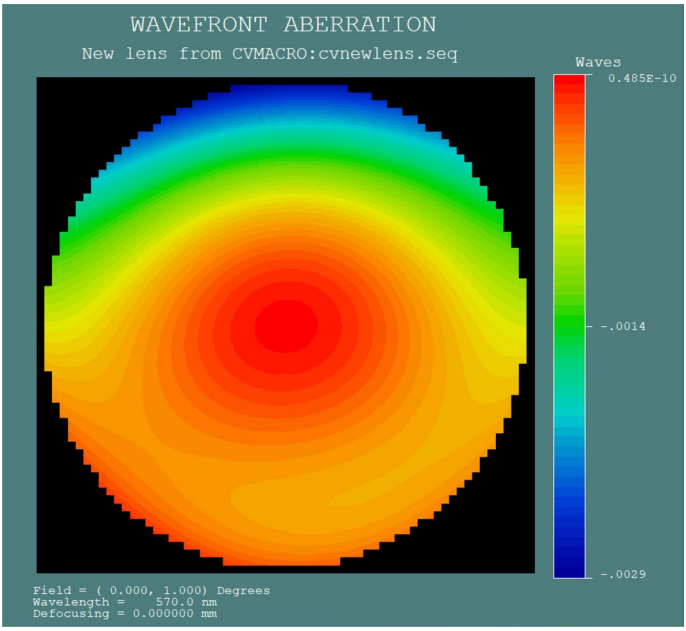

Fig. 14 Wavefront aberration diagram on image plane after astigmatism correction

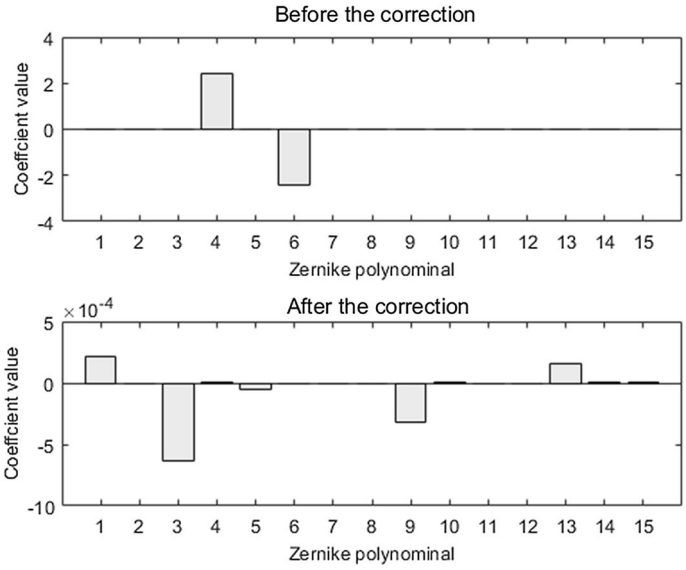

Fig. 15 Zernike coefficient changes before and after astigmatism calibration

uses an axicon to produce circular light, avoiding the central area of strong reflection, and can illuminate uniformly. The adaptive imaging system achieves the diffraction limit, and the MTF of each field of view at Nyquist is greater than 0.42, and the distortion is less than 0.15%. On the basis of the design, the experiment of simulating human astigmatism is carried out. Wavefront aberration is introduced into the pupil, and the results of wavefront correction are simulated by CODE V. The experiment shows that there is no additional aberration while correcting astigmatism, which provides an effective low-order compensation scheme for human astigmatism.

Funding Funding was provided by National Natural Science Foundation (NNSF) (61801455); Key Science and Technology Project of Jilin Science and Technology Department (20170204029GX). China Postdoctoral Science Foundation (2020M672053).

References

Chen, L., Kruger, P.B., Hofer, H., Singer, B., Williams, D.R.: Accommodation with higher-order monochromatic aberrations corrected with adaptive optics. JOSA A **23**(1), 1–8 (2006)

Chen, D.C., Jones, S.M., Silva, D.A., Olivier, S.S.: High-resolution adaptive optics scanning laser ophthalmoscope with dual deformable mirrors. JOSA A **24**(5), 1305–1312 (2007)

Fink, W., Micol, D.: simEye: computer-based simulation of visual perception under various eye defects using zernike polynomials. J. Biomed. Opt. **11**(5), 054011 (2006)

Fülep, C., Kovács, I., Kránitz, K., Erdei, G.: Simulation of visual acuity by personalizable neuro-physiological model of the human eye. Sci. Rep. **9**(1), 1–15 (2019)

Han, Y., Bryanston-Cross, P.J., Shaw, K., Hero, M.: Reflectivity of the human cornea and its influence on the selection of a suitable light source for a low-cost tonometer. In: Optics in Health Care and Biomedical Optics: Diagnostics and Treatment, vol. 4916, pp. 373–377. International Society for Optics and Photonics (2002)

Huanqing, G., Zhaoqi, W., Qiuling, Z., Wei, Q., Yan, W.: Eye model based on wavefront aberration measured subjectively. ACTA Photonica Sin. **34**(11), 1666 (2005)

Kaizu, Y., Nakao, S., Arima, M., Hayami, T., Wada, I., Yamaguchi, M., Sekiryu, H., Ishikawa, K., Ikeda, Y., Sonoda, K.H.: Flow density in optical coherence tomography angiography is useful for retinopathy diagnosis in diabetic patients. Sci. Rep. **9**(1), 1–7 (2019)

Krueger, M.L., Oliveira, M.M., Kronbauer, A.L.: Personalized visual simulation and objective validation of low-order aberrations of the human eye. In: 2016 29th SIBGRAPI Conference on Graphics, Patterns and Images (SIBGRAPI), pp. 64–71. IEEE (2016)

Ma, C., Cheng, D., Xu, C., Wang, Y.: Design, simulation and experimental analysis of an anti-stray-light illumination system of fundus camera. In: Optical Design and Testing VI, vol. 9272, p. 92720H. International Society for Optics and Photonics (2014)

Manny, R.E., Deng, L., Gwiazda, J., Hyman, L., Weissberg, E., Scheiman, M., Fern, K.D.: Internal astigmatism in myopes and non-myopes: compensation or constant? Optom. Vis. Sci. Off. Publ. Am. Acad. Optom. **93**(9), 1079–1092 (2016)

Niparugs, M., Tananuvat, N., Chaidaroon, W., Tangmonkongvoragul, C., Ausayakhun, S.: Outcomes of lasik for myopia or myopic astigmatism correction with the fs200 femtosecond laser and ex500 excimer laser platform. Open Ophthalmol. J. **12**, 63–71 (2018)

Ogagarue, E.R., Lutsey, P.L., Klein, R., Klein, B.E., Folsom, A.R.: Association of ideal cardiovascular health metrics and retinal microvascular findings: the atherosclerosis risk in communities study. J. Am. Heart Assoc. **2**(6), e000430 (2013)

Planchon, T.A., Mercere, P., Cheriaux, G., Chambaret, J.P.: Off-axis aberration compensation of focusing with spherical mirrors using deformable mirrors. Opt. Commun. **216**(1–3), 25–31 (2003)

Qin, Z., He, S., Yang, C., Yung, J.S.Y., Chen, C., Leung, C.K.S., Liu, K., Qu, J.Y.: Adaptive optics two-photon microscopy enables near-diffraction-limited and functional retinal imaging in vivo. Light Sci. Appl. **9**(1), 1–11 (2020)

Rioux, M., Tremblay, R., Belanger, P.A.: Linear, annular, and radial focusing with axicons and applications to laser machining. Appl. Opt. **17**(10), 1532–1536 (1978)
Sauders, H.: A method for determining the mean value of refractive errors. Br. J. Physiol. Opt. **34**, 1–11 (1980)
Smith, W.J.: Modern Optical Engineering. Tata McGraw-Hill Education, New York (2008)
Suliman, A., Rubin, A.: A review of higher order aberrations of the human eye. Afr. Vis. Eye Health **78**(1), 8 (2019)
Sun, Z., Feng, Y., Chen, Y., Shi, X.Y., Tan, Z.Y.: Research of adaptive optics system for correction human eye fundus imaging. In: 2012 International Conference on Wavelet Active Media Technology and Information Processing (ICWAMTIP), pp. 173–176. IEEE (2012)
Yau, J.W., Rogers, S.L., Kawasaki, R., Lamoureux, E.L., Kowalski, J.W., Bek, T., Chen, S.J., Dekker, J.M., Fletcher, A., Grauslund, J., et al.: Global prevalence and major risk factors of diabetic retinopathy. Diabetes Care **35**(3), 556–564 (2012)
Ye, H., Gao, Z., Qin, Z., Wang, Q.: Near-infrared fundus camera based on polarization switch in stray light elimination. Chin. Opt. Lett. **11**(3), 56–59 (2013)
Zhang, Y., Phan, E., Wildsoet, C.F.: Retinal defocus and form-deprivation exposure duration affects RPE BMP gene expression. Sci. Rep. **9**(1), 1–8 (2019)